Extracting signatures of quantum criticality in the finite-temperature behavior of many-body systems

Alessandro Cuccoli,[1] Alessio Taiti,[2] Ruggero Vaia,[3] and Paola Verrucchi[4,2]

[1] *Dipartimento di Fisica, Università di Firenze, e Unità CNISM, Via G. Sansone 1, I-50019 Sesto Fiorentino (FI), Italy*

[2] *Dipartimento di Fisica, Università di Firenze, Via G. Sansone 1, I-50019 Sesto Fiorentino (FI), Italy*

[3] *Istituto dei Sistemi Complessi – CNR, via Madonna del Piano 10, I-50019 Sesto Fiorentino (FI), Italy*

[4] *Centro di Ricerca e Sviluppo SMC dell'Istituto Nazionale di Fisica della Materia – CNR, Sezione di Firenze, via G. Sansone 1, I-50019 Sesto Fiorentino, Italy*

(Dated: February 1, 2008)

We face the problem of detecting and featuring footprints of quantum criticality in the finite-temperature behavior of quantum many-body systems. Our strategy is that of comparing the phase diagram of a system displaying a $T=0$ quantum phase transition with that of its classical limit, in order to single out the genuinely quantum effects. To this aim, we consider the one-dimensional Ising model in a transverse field: while the quantum $S=1/2$ Ising chain is exactly solvable and extensively studied, results for the classical limit ($S\to\infty$) of such model are lacking, and we supply them here. They are obtained numerically, via the Transfer-matrix method, and their asymptotic low-temperature behavior is also derived analytically by self-consistent spin-wave theory. We draw the classical phase-diagram according to the same procedure followed in the quantum analysis, and the two phase diagrams are found unexpectedly similar: Three regimes are detected also in the classical case, each characterized by a functional dependence of the correlation length on temperature and field analogous to that of the quantum model. What discriminates the classical from the quantum case are the different values of the exponents entering such dependencies, a consequence of the different nature of zero-temperature quantum fluctuations with respect to thermal ones.

I. INTRODUCTION

One of the most fascinating aspects of many-body systems is the possible occurrence of a phase transition, either at finite or at zero temperature. This latter case is generally referred to as a genuine *quantum* phase transition (QPT), by this meaning that it is exclusively observed in quantum many-body systems. Zero-point quantum fluctuations are recognized as the fundamental ingredient of a QPT, in the same sense as thermal fluctuations are in ordinary finite-temperature phase transitions: Whenever fluctuations are frozen, as in the $T=0$ classical case, no phase transition may possibly occur.

In the literature, a QPT is also commonly said to occur when, for a given value of one of the Hamiltonian parameters, the ground state of the model qualitatively changes its structure. This definition is not quite rigorous, firstly because it labels QPT any change in the universality class of the model, as well as mean-field phenomena such as saturation, secondly because it may paradoxically be extended to classical systems: As a matter of fact, qualitative changes in the structure of the minimum-energy configuration may well be observed, for a given value of some Hamiltonian parameter, also in classical systems at $T=0$, despite fluctuations being frozen. In this framework, therefore, the comparison between the behavior of a quantum system displaying a QPT and that of its classical limit becomes meaningful even at zero temperature, as shown in the next Section.

When temperature is switched on, the very same definition of QPT looses its meaning; however, it is well established that a QPT induces a peculiar finite-temperature behavior which is qualitatively described by the best known phase diagram introduced in Ref. 1, and reported in Fig. 7, where three different regimes appear (*renormalized classical*, *quantum critical*, and *quantum disordered*), separated by crossover lines thoroughly discussed in Ref. 2. The relevance of this phase diagram is mostly due to its suggesting that signatures of a genuine quantum critical behavior may survive also at finite temperature, a fact that opens the possibility to observe them experimentally. Moreover, a renewed interest has arisen since entanglement properties have entered the physics of many-body systems, and questions like "how resistant to thermal noise are certain quantum properties?" became essential in order to test possible realizations of quantum devices.

Despite the above phase diagram being considered as strictly peculiar to quantum systems, especially as far as the quantum critical and quantum disordered regimes are concerned, its structure results from the interplay between thermal (*classical*) and *quantum* fluctuations: A precise analysis of the role played by these two components is therefore necessary in order to ascertain whether the latter play an essential role or not, and to distill genuine footprints of quantum criticality to be experimentally looked for. To this end, knowing the behavior of the quantum system at finite temperature is not enough, and a careful comparison with the corresponding classical limit is necessary. The quite unexpected lack of results for the classical limit of quantum models displaying a QPT has made such comparison unavailable until now.

This paper is aimed at filling this gap: We consider one of the paradigmatic models displaying a QPT, namely

the one-dimensional quantum Ising model in a transverse field (QIF), and compare its behavior with that of its classical limit, namely the classical Ising model in a transverse field (CIF), which we study numerically, via the Transfer-matrix method, and analytically, via self-consistent spin-wave theory. The result is unexpected: A finite temperature phase diagram is disclosed also for the CIF, and it has the same structure of that for the QIF. In full analogy with the quantum case, we identify three different regimes on the basis of the field and temperature dependence of the correlation length; moreover, we show that the algebraic behavior, which was thought to specifically characterize the quantum critical and quantum disordered regimes, does in fact show up also in the classical system, though with different exponents. This result jeopardizes the experimental renderings based on the statement that the observation of an algebraic dependence of the correlation length implies the occurrence of a quantum critical or disordered regime[3,4,5,6]. In fact, an accurate analysis of the exponents is here shown to be necessary in order to discriminate genuine quantum effects.

The structure of the paper is as follows: in Sec. II we introduce the model and discuss its zero-temperature behavior. In Sec. III, we first summarize the known results for the QIF, and then present our results for its classical limit, the CIF: numerical data for the magnetization and the susceptibility in the field direction, and for the specific heat are shown and discussed. The analysis of the field and temperature dependence of the correlation length is considered in Sec. IV, where the classical phase diagram is finally obtained and compared with that for the QIF. Conclusions are drawn in Sec. V.

II. THE ISING MODEL IN A TRANSVERSE FIELD: $T = 0$

A. The quantum model

One of the best known examples of a many-body system displaying a QPT[2,7] is the one-dimensional quantum Ising model in a transverse field (QIF), whose Hamiltonian reads

$$\frac{\hat{\mathcal{H}}}{J} = -\sum_i \left(\hat{S}_i^x \hat{S}_{i+1}^x + H\, \hat{S}_i^z \right) , \qquad (1)$$

where i runs over the sites of an infinite chain, and $\hat{\boldsymbol{S}}_i$ are S=1/2 spin operators, J is the exchange energy constant and H is the transverse field in units of J; this model is exactly solvable[8,9] by means of a Jordan-Wigner transformation to Fermi operators, and displays a QPT at $T = 0$ and $H = H_{\rm c} = 1/2$: The discrete $\hat{S}_i^x \to -\hat{S}_i^x$ global symmetry of the Hamiltonian is spontaneously broken for $H < H_{\rm c}$, where the order parameter $m_x = \langle \hat{S}_i^x \rangle / S$ becomes nonzero; long-range order sets in at the critical point, as testified by the divergence of the order-parameter correlation length. In particular, it is

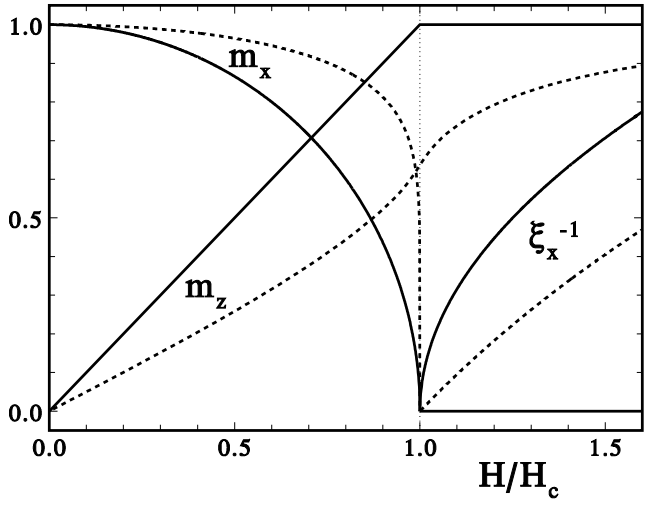

FIG. 1: Zero temperature limit of m_x, m_z, and ξ_x of the classical (solid lines) and of the quantum (dashed lines) Ising model in a transverse field.

$$m_x \sim (H_{\rm c} - H)^{\beta} \quad \text{for } H \to H_{\rm c}^- , \qquad (2)$$

and

$$\xi_x \sim (H - H_{\rm c})^{-\nu} \quad \text{for } H \to H_{\rm c}^+ , \qquad (3)$$

with the exponents $\beta = 1/8$ and $\nu = 1$, as in the finite-temperature phase transition of the classical two-dimensional Ising model.[10] Together with the other usual exponents they obey typical scaling relations which, due to the intrinsically dynamical nature of quantum fluctuations, entail[2] the dynamical critical exponent z. On the other hand, the magnetization along the field direction, $m_z = \langle \hat{S}_i^z \rangle / S$, is an analytic function of the field and changes its curvature at $H_{\rm c}$, where the uniform susceptibility consequently displays a maximum. These $T = 0$ behaviors are reported as dashed lines in Fig. 1.

B. The classical model

The classical limit of any given quantum system is unique, although the converse is not true. For a spin system the limit $\hbar \to 0$ must be taken while keeping finite the spin angular momenta $\hbar \hat{\boldsymbol{S}}_{\boldsymbol{i}}$.

From Eq. (1) one thus obtains the Hamiltonian of the classical Ising model in a transverse field (CIF),

$$\frac{\mathcal{H}}{J_{\rm c}} = -\sum_{i=1}^{N} \left(s_i^x s_{i+1}^x + 2h\, s_i^z \right) . \qquad (4)$$

where $\boldsymbol{s}_i = (s_i^x, s_i^y, s_i^z)$ are *classical spins*, i.e., three-dimensional vectors of fixed length $|\boldsymbol{s}_i|^2 = 1$, while[11]

$$J_{\rm c} = \lim_{\substack{\hbar \to 0 \\ S \to \infty}} JS^2 , \qquad 2h = \lim_{\substack{\hbar \to 0 \\ S \to \infty}} \frac{H}{S}$$

are the classical exchange interaction and reduced field, respectively. Taking the exchange interaction as the energy unit, the dimensionless temperature will be denoted with $t = T/J_c$, so that all thermodynamic quantities depend upon the pair (h,t). Periodic boundary conditions are assumed ($\boldsymbol{s}_{N+1} = \boldsymbol{s}_1$) and the thermodynamic limit ($N \to \infty$) will be considered.

It is important to distinguish between the CIF and what is often called the *classical Ising model*, which is obtained from Eq. (1) with $H = 0$, by regarding the quantum operators $\hat{S}_i^x$ as classical discrete variables taking the values $\pm 1/2$. Results for the CIF are lacking, apart from the zero-field case[12,13,14], probably because, at variance with the QIF, the CIF does not allow for an exact solution.

Writing the classical spin variables in terms of polar angles as

$$\boldsymbol{s}_i \equiv \left(\sin\theta_i, \cos\theta_i \sin\varphi_i, \cos\theta_i \cos\varphi_i \right) , \qquad (5)$$

the Hamiltonian (4) is expressed as

$$\frac{\mathcal{H}}{J_c} = -\sum_i \left(\sin\theta_i \sin\theta_{i+1} + 2h \cos\theta_i \cos\varphi_i \right) ; \qquad (6)$$

its minimum corresponds to a translation-invariant configuration $\left\{ \boldsymbol{s}_i = \left(\sin\theta_m, 0, \cos\theta_m \right) \right\}$, with

$$\theta_m(h) = \begin{cases} \pm \cos^{-1} h & \text{for } h \le 1 \\ 0 & \text{for } h \ge 1 \end{cases} . \qquad (7)$$

The minimum energy per spin is

$$u(h,0) = \begin{cases} -1 - h^2 & \text{for } h \le 1 \\ -2h & \text{for } h \ge 1 \end{cases} \qquad (8)$$

and shows a singularity at $h = 1$. The magnetization m_z is proportional to the field for $h \le 1$ and saturates for $h \ge 1$,

$$m_z(h,0) = \begin{cases} h & \text{for } h \le 1 \\ 1 & \text{for } h \ge 1 \end{cases} , \qquad (9)$$

so that the corresponding susceptibility is discontinuous at $h = 1$

$$\chi_z(h,0) = \partial_h m_z = \begin{cases} 1 & \text{for } h < 1 \\ 0 & \text{for } h > 1 \end{cases} . \qquad (10)$$

Finally, the behavior of the magnetization along the exchange,

$$m_x(h,0) = \begin{cases} \pm\sqrt{1-h^2} & \text{for } h \le 1 \\ 0 & \text{for } h \ge 1 \end{cases} , \qquad (11)$$

reflects the fact that for $h < 1$ the minimum is twofold.

It may sound odd but, as seen in Fig. 1, the CIF displays a zero-temperature behavior which is analogous to that observed in the QIF, even if no fluctuations are present at $t = 0$. Eq. (11) shows indeed that a *critical* field, $h_c = 1$, separates a symmetry-broken minimum-energy configuration with $m_x \neq 0$ from one with $m_x = 0$.

An even closer analogy is found if one considers that from the low-temperature expression derived in Appendix B one can obtain the exact zero-t limit of the correlation length, $\xi_x(h,0) = 1/\sqrt{h-1}$. The counterparts of both Eqs. (2) and (3) are then available, and read

$$m_x \sim (h_c - h)^\beta \quad \text{for } h \to h_c^- , \qquad (12)$$

and

$$\xi_x \sim (h - h_c)^{-\nu} \quad \text{for } h \to h_c^+ , \qquad (13)$$

with Gaussian critical exponents $\beta = \nu = 1/2$, to be compared with those for the QIF, $\beta = 1/8$ and $\nu = 1$.

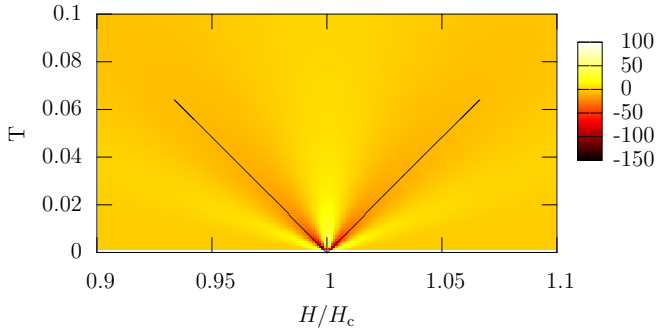

FIG. 2: Second derivative of the specific heath of the QIC, $\partial_H^2 c(H,T)$.

III. THE ISING MODEL IN A TRANSVERSE FIELD : $T > 0$

A. $T > 0$: The quantum model

The field- and temperature dependence of the specific heat $c(H,T)$ and of the susceptibility $\chi_z(H,T)$ can be easily obtained from the analytic results of Ref. 9. The most prominent feature is the occurrence of maxima of both quantities in the $H-T$ plane. Indeed, the quantum specific heat just shows the behavior of a free Fermi gas with dispersion $\omega_k \sim \Delta + k^2$ in the neighborhood of a vanishing gap $\Delta \sim |H - H_c|$, which appears, for fixed low-T, as two symmetric peaks at linearly displaced positions $|H - H_c| \propto T$. This feature is made evident in Fig. 2, by the density plot of the second derivative of $c(H,T)$ with respect to H. The positions of the maxima draw two symmetric lines in the $H - T$ plane which coincide with those obtained[15] from the analysis of entanglement properties.

B. $T > 0$: The classical model

The thermodynamic behavior of the CIF for $h < h_c$ is essentially determined by the energy landscape of

the model. In a mean-field approach, i.e., setting $\{\theta_i = \theta, \varphi_i = 0\}$, this is described by the double-well energy profile $e(\theta) = -\sin^2\theta - 2h\cos\theta$, with minima in $\theta_{\rm m} = \pm\cos^{-1} h$ and the barrier top at $\theta = 0$, the barrier energy being $\delta e = (1-h)^2 = (h_{\rm c}-h)^2$. The two wells correspond to the Ising configurations.

Domain-wall excitations connecting the two Ising configurations can appear on the chain, the energy of a domain wall being $e_{\rm w} = 2(1-h^2)$. A simple statistical argument gives a finite number of domain walls at any finite temperature, $n_{\rm w} \sim N/(1+e^{e_{\rm w}/t})$, so that when temperature is switched on the ordered state is destroyed (i.e., $m_x = 0$ for $t > 0$) by these excitations, which rule the low-temperature thermodynamics in what we will hereafter call the *Ising* regime.

When the temperature reaches the order of the barrier energy, $t \sim (h_{\rm c}-h)^2$, thermally activated transitions between the wells can occur and the Ising regime breaks down. The dependence of the barrier height on the field is responsible for the fact that as $h \to h_{\rm c}^-$ this regime gets confined into the narrow interval $0 < t < (h_{\rm c}-h)^2$. The above mechanism, that we call *thermal hopping*, is at the hearth of the phenomenology of the model below $h_{\rm c}$, and it already suggests the occurrence of a crossover from an Ising-like behavior towards a *critical* one, ruled by an effectively flat energy-landscape.

On this basis, let us discuss the finite-temperature data obtained[16] by the Transfer-matrix method, briefly described in Appendix A.

The temperature behavior of the magnetization along the field, $m_z(h,t)$, is shown in Fig. 3, and clearly is related to that of the mean-square fluctuations of the Ising order parameter, $\langle (s_i^x)^2 \rangle$; indeed, the initial increase with temperature corresponds to the reduction of $\langle (s_i^x)^2 \rangle$ due to the fact that the probability distribution of s_i^x, initially frozen in the bottom of one of the two wells ($\pm\sqrt{1-h^2}$), extends more likely towards the barrier at $s_i^x = 0$. The further decay of m_z is due to the isotropic spin fluctuations occurring after thermal hopping has taken place. On the other hand, for $h \geq h_{\rm c}$, m_z simply decreases from its $t = 0$ saturation value.

The susceptibility $\chi_z(h,t)$ is shown in Fig. 4: the zero-field result agrees with that derived in Ref. 13 and shows a broad maximum in temperature, at $t \simeq 0.37$. Upon rising the field, such maximum is squeezed towards lower temperatures, meanwhile getting sharper. At the critical field, the maximum disappears and the susceptibility is a monotonic function of temperature for whatever $h \geq h_{\rm c}$. The zero-t limiting value of $\chi_z(h,t)$ is given by Eq. (10). The overall behavior of $\chi_z(h,t)$ in the h–t plane is evidently characterized by the occurrence of the above described maxima for $h < h_{\rm c}$.

The specific heat $c(h,t)$, shown in Fig. 5, is also characterized by the occurrence of maxima for $h < h_{\rm c}$, which disappear above the critical field; noticeably they fall into almost the same positions as those observed in $\chi_x(h,t)$, as it appears in Fig. 6.

The maxima observed both in the susceptibility and in

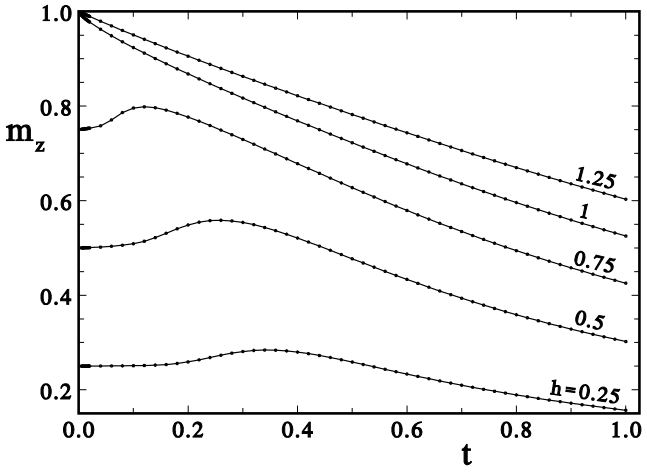

FIG. 3: Magnetization along the field direction, $m_z(h,t)$ *vs* temperature, for selected field values. The 'critical' value is $h_{\rm c} = 1$.

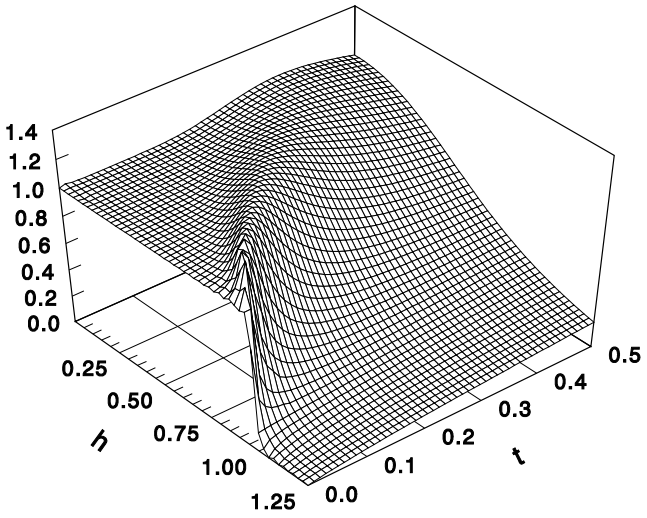

FIG. 4: Magnetic susceptibility $\chi_z(h,t)$.

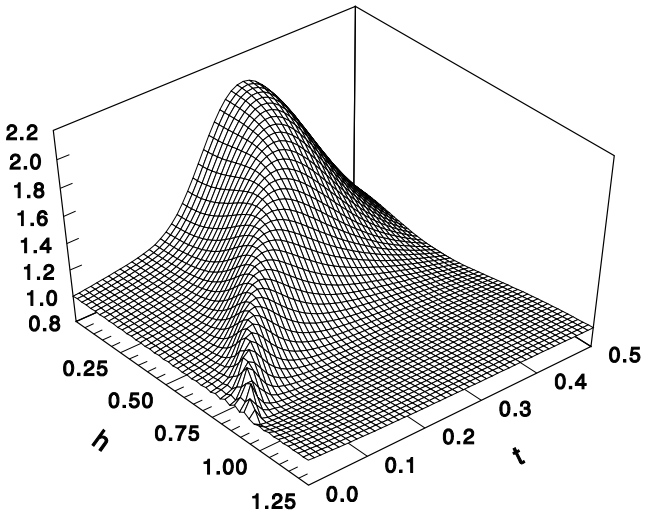

FIG. 5: Specific heat $c(h,t)$.

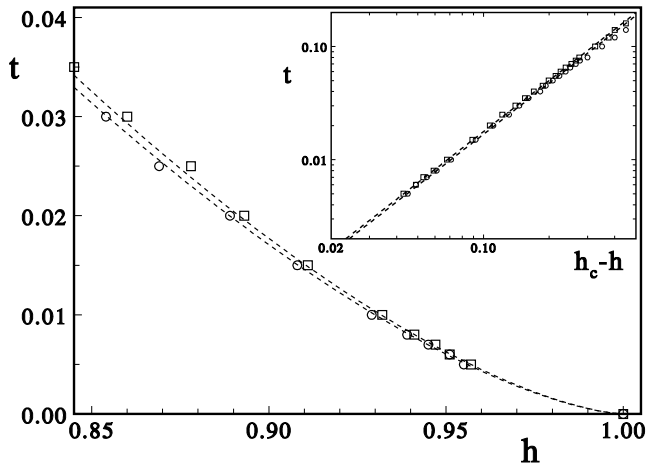

FIG. 6: Region $h \lesssim h_c$ of the phase diagram of the CIF. Circles and squares indicate the position of the maxima of $c(h,t)$ and $\chi(h,t)$, respectively. The dashed curves are obtained fitting the data with $t \propto (1-h)^{3/2}$. Inset: log-log plot of the same data and curves.

the specific heat correspond to the onset of thermal hopping, and their positions indicate the region where thermal fluctuations overcome the Ising domain-wall energy, i.e., the crossover region from the *Ising* to the *critical* regime. In order to better characterize the corresponding crossover line we have fitted the maxima positions for low t in the h–t plane with the function $t \propto (h_c - h)^{\kappa}$, finding the exponent quite close to the value $\kappa = 3/2$ derived by analytical arguments in the next section.

IV. THE PHASE DIAGRAM

A. Quantum model

The finite-temperature phase diagram for the QIF, shown in Fig. 7, essentially features the occurrence of three regions, characterized by qualitatively different behavior of physical observables with respect to h and t. These regions have been identified[1] with the so called *renormalized-classical* (**A**), *quantum-critical* (**B**), and *quantum-disordered* (**C**) regimes, which have been singled out according to the qualitatively different behavior of the correlation length ξ_x, which is

$$\xi_x \sim \begin{cases} e^{u(H_c - H)/T} & \text{for } H_c - H \gg T \quad (\mathbf{A}) \\ T^{-1/y} & \text{for } |H - H_c| \ll T \quad (\mathbf{B}) \\ (H - H_c)^{-\nu} & \text{for } H - H_c \gg T \quad (\mathbf{C}) \end{cases} \qquad (14)$$

where u is a constant and the critical exponents are $y = 1$ and $\nu = 1$. The power law divergence in Eqs. (14)-(**B**) and -(**C**) follow from the temperature-dependent scaling law for ξ_x lying at the hearth of the Renormalization Group (RG) approach to critical phenomena[2,7]. We remind that the exponent y, ruling the scaling of energy, is bound to equal the dynamical critical exponent z by the uncertainty principle. In the same framework, the above regimes are shown to be separated by the crossover lines $T \propto |H - H_c|$.

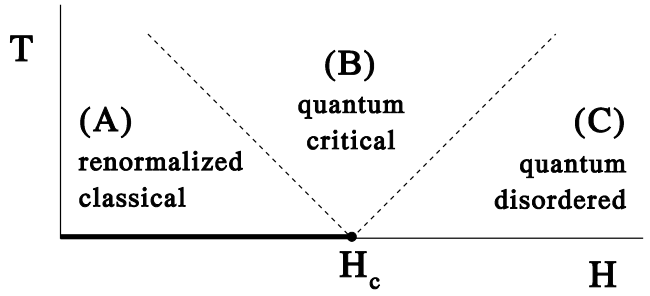

FIG. 7: Phase diagram of the quantum Ising model in a transverse field.

This phase-diagram has been extensively discussed (see, e.g., Refs. 7 and 2) over the last decade: in particular, the fact that ξ_x is independent of the field and inversely proportional to T in region **B**, and independent of temperature and inversely proportional to $H - H_c$ in region **C**, has always been considered as a signature of the genuinely quantum character of the corresponding regimes, which have consequently been labeled as "quantum" (critical and disordered, respectively).

In fact, as we argue in the remaining part of this article, this is not truly the case.

B. Classical model

As seen in Sec. III B, hints of the possible occurrence of at least two different regimes, separated by a crossover region, do already come from the behavior of the susceptibility and of the specific heat for $h < h_c$. However, in order to closely mimic the procedure followed in drawing the quantum phase diagram, we analyze the field and temperature dependence of the correlation length $\xi_x(h,t)$ of the classical model, heading towards expressions analogous to those of Eqs. (14). The overall behavior of $\xi_x(h,t)$, as from our numerical data, is plotted in Figs. 8 and 9.

1. *Correlation length for $h < h_c$*

If one considers the t-dependence for $h < h_c$, it clearly appears from Fig. 8 that $\ln \xi_x \propto 1/t$, with a slope that increases with the difference $h_c - h$. As for the field dependence, the logarithm of $\xi_x(h,t)$ is seen in Fig. 9 to be linear in h, with negative slope: this is the more evident the smaller the temperature and the angular coefficient decreases with increasing t, consistently with Eq. (14)-(**A**). In fact, from Fig. 10 for $h_c - h \gg t$ we see that $t \ln \xi_x(h,t) \approx f(t) + a(h_c - h)$, with $f(t)$ weakly dependent on t, meaning

$$\xi_x(h,t) \sim e^{u(h_c - h)/t} \quad \text{for } h_c - h \gg t \quad (\mathbf{a}). \qquad (15)$$

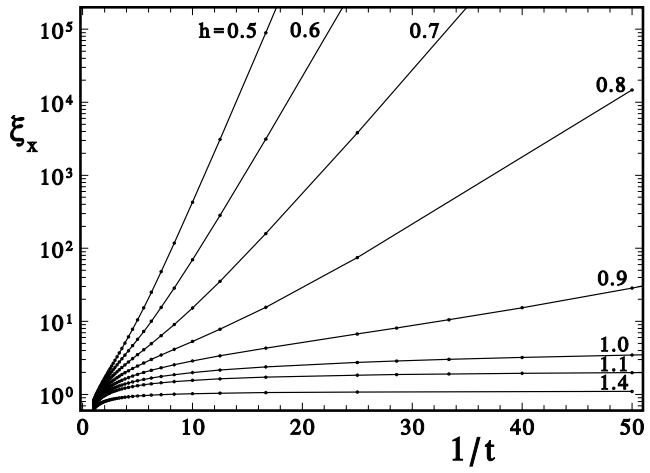

FIG. 8: Correlation length $\xi_x(h,t)$ *vs* $1/t$, for selected field values.

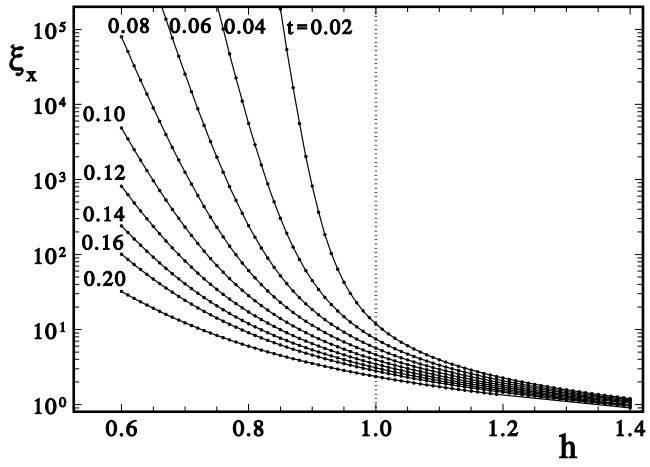

FIG. 9: Correlation length $\xi_x(h,t)$ *vs* field, for different temperatures.The vertical dotted line marks the critical field $h_c = 1$.

2. *Correlation length for $h \geq h_c$*

From Figs. 8 and 9 we see that for field close and above the critical value, the temperature- and field dependence of $\xi_x(h,t)$ becomes much less pronounced with respect to those displayed below the critical field, suggesting power-law behaviors of the same type observed in the quantum regimes **B** and **C**.

In particular, using our numerical data, we can ascertain that, for $|h-h_c| \ll t$ the correlation length behaves as $\xi_x \propto t^{-1/3}$, as evidenced in Fig. 11; on the other hand, for $|h-h_c| \gg t$, the log-log plot reported in Fig. 12 emphasizes a power-law field-dependence, $\xi_x \propto (h-h_c)^{-1/2}$. These behaviors are fully analogous to the quantum ones described by Eq. (14)-(**B**) and -(**C**), the only difference being in the exponents.

In order to strengthen this result, we develop the analytical treatment reported in Appendix B, which

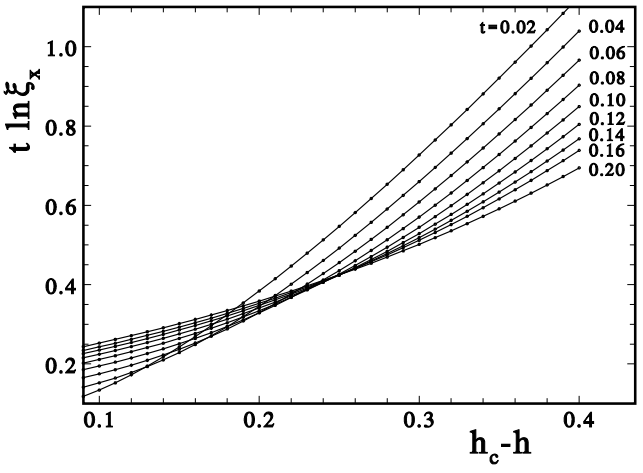

FIG. 10: Classical phase-diagram region **a**. The function $t \ln \xi_x(h,t)]$ vs $h_c - h$ for different fixed temperatures. One can see that the curves become straight lines the better the condition $h_c - h \gg t$ is satisfied.

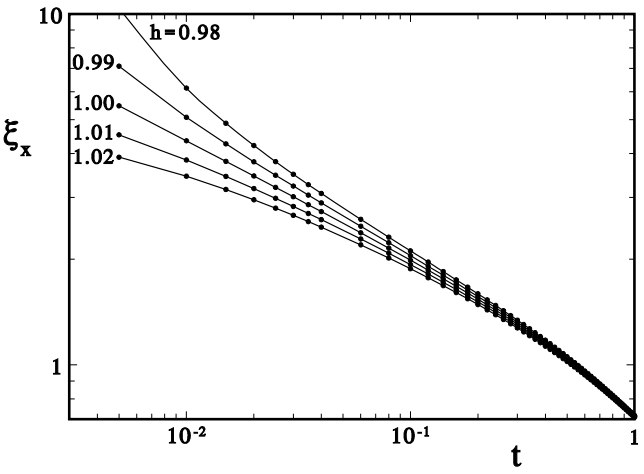

FIG. 11: Classical phase-diagram region **b**. Longitudinal correlation length $\xi_x(h,t)$ vs t for fields close to the critical value $h_c = 1$. The log-log plot emphasizes that the slope of the curve for $h = h_c$ is -1/3.

makes use of self-consistent spin-wave theory (SSWT) for $h \geq h_c$. The asymptotic behavior of the correlation length derived there, valid at low temperature and close to criticality, is given by Eq. (B9) and yields

$$\xi_x(h,t) \sim t^{-1/3} \qquad \text{for} \quad |h-h_c| \ll t \quad (\mathbf{b}), \qquad (16)$$

and

$$\xi_x(h,t) \sim (h-h_c)^{-1/2} \quad \text{for} \quad |h-h_c| \gg t \quad (\mathbf{c}), \qquad (17)$$

in full agreement with the analysis of our numerical data.

3. *Crossovers*

Let us now consider the problem of identifying the crossover regions between phases where Eqs. (15), (16),

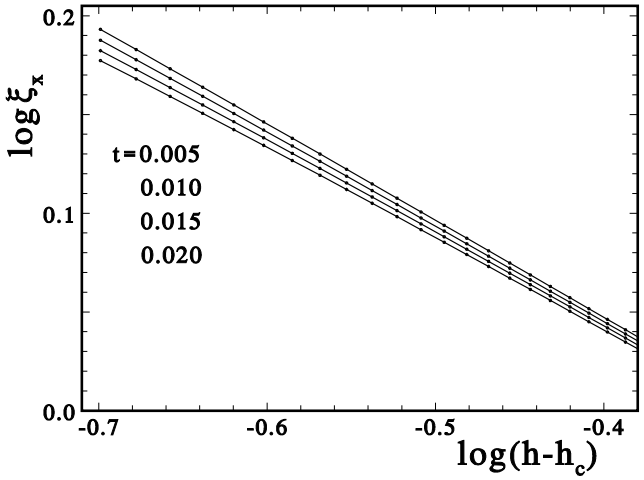

FIG. 12: Classical phase-diagram region **c**. Log-log plot of $\xi_x(h,t)$ vs $h-h_c$, for different low temperatures. The slope of the low-t curves is seen to be -1/2.

and (17) hold, i.e., between the three classical regimes, that we have labeled **a**, **b**, and **c**, respectively.

As for the **ab** crossover, a reasonable localization can be obtained by relating it with thermal hopping. According to the mean-field analysis presented in Sec. III B, the latter occurs when the temperature overcomes the energy-barrier height, i.e., for $h_c - h \sim t^{1/2}$. However, the mean-field approach neglects correlated fluctuations, while to get a correct estimate it is necessary to keep nearest-neighbor fluctuations at least within a quadratic approximation of the Hamiltonian (6) around one of the minima. Setting $\theta_i = \theta_m + \varepsilon_i$ and expanding, one finds for the quadratic part

$$\frac{\mathcal{H}}{J_c} \simeq N\, e(\theta_m) + h^2 \sum_k \varphi_k^2 + \sum_k (1 - h^2 \cos k)\, \varepsilon_k^2 \ , \quad (18)$$

from which the mean square fluctuation of θ_i around the minimum results

$$\langle \varepsilon_i^2 \rangle \simeq \frac{t}{2N} \sum_k \frac{1}{1 - h^2 \cos k} = \frac{t}{2\sqrt{1-h^4}} \ . \quad (19)$$

As soon as these fluctuations reach the size of the width of the barrier, $|\theta_m| = \sin^{-1}\sqrt{1-h^2}$, the Ising excitations disappear and the crossover between the exponential- and the power-law correlation length is expected. This condition is fulfilled when $\langle \varepsilon_i^2 \rangle \simeq |\theta_m|^2$, i.e., for h close to the critical field $h_c = 1$,

$$t \sim (h_c - h)^{3/2} \qquad (\mathbf{ab}) \ . \quad (20)$$

This prediction gives the correct exponent and is also fully consistent with that obtained in Sec. III B by fitting the positions of the maxima observed, in the $h-t$ plane, for both the susceptibility and the specific heat.

It is worth mentioning that thermal hopping is the ultimate cause of the finite-temperature phase transition to the ordered state occurring for $h < h_c$ in more than one dimension: the crossover turns indeed into the sharp critical line $t_c(h)$, with the critical temperature vanishing at the quantum critical point, $t_c(h_c) = 0$. In one dimension the onset of ordering is forbidden at finite t and only the broad crossover between regimes **a** and **b** survives.

Coming to the **bc** crossover, from Eqs. (16) and (17) one deduces it to occur for

$$t \sim (h - h_c)^{3/2} \qquad (\mathbf{bc}) \ . \quad (21)$$

4. *Phase diagram*

Eqs. (15), (16), and (17), can be summarized as:

$$\xi_x \sim \begin{cases} e^{u(h_c - h)/t} & \text{for } \ h_c - h \gg t \quad (\mathbf{a}) \\ t^{-1/y} & \text{for } |h - h_c| \ll t \quad (\mathbf{b}) \\ (h - h_c)^{-\nu} & \text{for } \ h - h_c \gg t \quad (\mathbf{c}) \end{cases} \quad (22)$$

with $y = 3$ and $\nu = 1/2$. Via the different behavior of the correlation length, three different regimes can thus be singled out also in the classical phase diagram and, according to our discussion, it makes sense to call them *Ising* (**a**), *critical* (**b**), and *disordered* (**c**). Different regimes are again separated by crossover lines, which in the classical model are described by the relation $t \sim |h - h_c|^{3/2}$.

C. Classical vs quantum phase diagram

Eqs. (22) clearly show that the CIF is characterized by a phase diagram on the $h-t$ plane which is fully analogous to the celebrated quantum one described by Eqs. (14). In particular, the observed power-law divergence of ξ_x in regimes (**b**) and (**c**) suggests the scaling hypothesis to hold also in the classical case: This is confirmed in Appendix B where we obtain an explicit expression for $\xi_x(h,t)$, which turns out to be a homogeneous function.

The nexus between the quantum and the classical case can be drawn as follows: Let us introduce the unifying parameters $\overline{g}$ and $\overline{t}$, defined as $\overline{g} = H - H_c$, $\overline{t} = T/J$ in the quantum model, and $\overline{g} = h - h_c$, $\overline{t} = t$ in the classical model, and write the equation

$$\xi_x(\overline{g}, \overline{t}) = b\, \xi_x\big(b^{1/\nu}\overline{g}, b^y\, \overline{t}\big) \quad (23)$$

which, within RG, rules the scaling of observable quantities and model parameters in the proximity of critical points after a length-scale transformation by a factor b. From Eq. (23) follow both the quantum Eqs. (14)-(**B**) and -(**C**) and the classical ones, (22)-(**b**) and -(**c**), as well as the crossover lines $\overline{t} \propto \overline{g}^{\nu y}$: The critical exponents entering the above expressions, despite getting different values in the quantum ($y = 1, \nu = 1$) and in the classical ($y = 3, \nu = 1/2$) case, consistently fulfil the hyperscaling relation

$$2 - \alpha = \nu(d + y) \ , \quad (24)$$

where $2-\alpha$ is the exponent for free-energy density f, defined[2] by $f(\overline{g},0)\sim|\overline{g}|^{2-\alpha}$ ($\alpha=0$ in both cases). We remind that, in the quantum case, the scaling exponent of energy y is unavoidably related to the dynamical critical exponent z by the uncertainty relation, $y=z$. As for the classical case, we notice that ν takes the typical Gaussian value, due to fluctuations freezing as $t\to 0$.

V. CONCLUSIONS

In this paper we have compared the finite-temperature phase diagram of a quantum model displaying a QPT, namely the $S=1/2$ Ising chain in a transverse field, with that of its classical limit. To this end, we have obtained numerical and analytical results for the classical model. In particular, we have studied the magnetizations, the specific heat, the magnetic susceptibility, and the correlation length along the exchange direction: all quantities have been analyzed below, at, and above the saturation field, with the temperature raised from zero up to values of the order of the exchange interaction.

The classical phase diagram emerging from our work is fully analogous to that of the quantum model. Three regimes are identified: the *Ising* regime **a** ($h_{\rm c}-h\gg t$), corresponding to the quantum *renormalized classical* regime, where ξ_x behaves exponentially with $(h_{\rm c}-h)/t$; the *critical* regime **b** ($|h-h_{\rm c}|\ll t$), corresponding to the *quantum critical* regime, where ξ_x behaves algebraically with t; the *disordered* regime **c** ($h-h_{\rm c}\gg t$), corresponding to the *quantum disordered* regime, where ξ_x behaves algebraically with $h-h_{\rm c}$. Two crossover lines, $t\sim|h-h_{\rm c}|^{3/2}$, separate the regions of the phase diagram where the above regimes occur.

The essential message of this work is that in order to discriminate quantum critical effects it is not sufficient to observe, say, an algebraic behavior of the correlation length with respect to temperature, but a precise determination of the exponent is rather due. Our analysis does also suggest that the role of genuinely quantum fluctuations at finite temperature is not as relevant as commonly believed, given the fact that most of the features regarded as typical of the quantum model are disclosed also in its classical limit, even, and most noticeably, at very low temperature.

Given the very weak model-dependence of the overall discussion, we believe that the above conclusions hold in general, and not only for the Ising chain in a transverse field.

We gratefully acknowledge fruitful discussions with A. Fubini. This work was supported by MIUR under the 2005-2007 PRIN–COFIN National Research Projects Program, n. 2005029421_004.

APPENDIX A: TRANSFER-MATRIX FOR THE CIF

We outline here the numerical Transfer-matrix technique,[17] by which we have investigated different static thermodynamic quantities of the CIF, focusing the attention on their low-temperature behavior in the neighborhood of the point $h=h_{\rm c}$.

Using polar coordinates one can map the classical spins appearing in the Hamiltonian (4) as

$$\boldsymbol{s}_i=\left(x_i,\sqrt{1-x_i^2}\sin\varphi_i,\sqrt{1-x_i^2}\cos\varphi_i\right)\ , \qquad \text{(A1)}$$

with $x_i\in[-1,1]$ and $\varphi_i\in[0,2\pi]$. The partition function can then be expressed as the trace of the N-th power of an integral kernel $K(x,y)$,

$$\begin{aligned}\mathcal{Z} &= \prod_{i=1}^{N}\int_{-1}^{1}\frac{dx_i}{2}\int_{-\pi}^{\pi}\frac{d\varphi_i}{2\pi}\,e^{(x_ix_{i+1}+2h\sqrt{1-x_i^2}\cos\varphi_i)/t}\\ &= \int_{-1}^{1}dx\ K^N(x,x)=\sum_\ell\lambda_\ell^N\ , \qquad \text{(A2)}\end{aligned}$$

where the kernel is real and symmetric,

$$\begin{aligned}K(x,y) &= \frac{e^{xy/t}}{2}\left[I_0\left(\tfrac{2h}{t}\sqrt{1-x^2}\right)I_0\left(\tfrac{2h}{t}\sqrt{1-y^2}\right)\right]^{\frac{1}{2}}\\ &= \sum_\ell\lambda_\ell\,\psi_\ell(x)\psi_\ell(y)\ , \qquad \text{(A3)}\end{aligned}$$

$I_0(x)$ is the modified Bessel function, $\{\lambda_\ell\}=\{\lambda_0,\lambda_1,...\}$ are the (positive) eigenvalues of K (say, in decreasing order), and $\{\psi_\ell(x)\}$ the corresponding (real) eigenfunctions. The diagonalization of K was performed numerically after discretizing the integral with a 5-point Simpson's formula[18] on a mesh of up to 1040 intervals, also accounting for the definite parity of the eigenfunctions.

In the thermodynamic limit the free energy per site is a function of the largest eigenvalue only,

$$f(h,t)=-t\lim_{N\to\infty}\frac{1}{N}\ln\mathcal{Z}_N=-t\ \ln\lambda_0(h,t)\ ; \qquad \text{(A4)}$$

the internal energy $u=t^2\partial_t\ln\lambda_0$ and the specific heat $c=\partial_t u$, were obtained by numerical differentiation (5-point Lagrange formula[18]).

The probability distribution for the variable $x=x_i$ is

$$w(x)=\psi_0^2(x)\ ; \qquad \text{(A5)}$$

one can reduce to averages with this probability both the expressions for the magnetization along the field $m_z=\langle s_i^z\rangle=(t/2)\partial_h\ln\lambda_0$ and for the corresponding susceptibility $\chi_z=\partial_h m_z$. On the other hand, the joint probability for two sites at a distance r, $x=x_i$ and $y=x_{i+r}$, is

$$w_r(x,y)=\sum_\ell\left(\frac{\lambda_\ell}{\lambda_0}\right)^r\psi_0(x)\psi_\ell(x)\psi_0(y)\psi_\ell(y). \qquad \text{(A6)}$$

Using this result, one can write the correlation function of the spin components in the direction of the exchange as

$$\langle s_i^x s_{i+r}^x\rangle = \sum_\ell \Big[\int dx\ x\,\psi_0(x)\psi_\ell(x)\Big]^2 \Big(\frac{\lambda_\ell}{\lambda_0}\Big)^r\ ; \quad \text{(A7)}$$

as the eigenfunction $\psi_0(x)$ is even, for large r the leading term is that for $\ell=1$,

$$\langle s_i^x s_{i+r}^x\rangle \underset{r\to\infty}{\sim} \Big(\frac{\lambda_1}{\lambda_0}\Big)^r\ , \quad \text{(A8)}$$

so that the corresponding correlation length is given by

$$\xi_x(h,t) = \big[\ln(\lambda_0/\lambda_1)\big]^{-1}\ . \quad \text{(A9)}$$

APPENDIX B: SELF-CONSISTENT SPIN-WAVE THEORY

For $h \geq h_{\rm c}$ the minimum configuration of the classical Hamiltonian Eq. (6) corresponds to the saturation one, i.e., $\{\theta_i=0,\varphi_i=0\}$. In order to estimate the low-temperature behavior of the correlation length, we use self-consistent spin-wave theory (SSWT), i.e., we assume a Gaussian distribution $\rho_0 = e^{-\beta\mathcal{H}_0}$ in terms of a trial quadratic Hamiltonian $\mathcal{H}_0$ whose coefficients are self-consistently determined by requiring the identity of the ρ_0 averages of $\mathcal{H}$ and $\mathcal{H}_0$, as well as of their first and second derivatives.

In terms of the relevant Gaussian variances $D=\langle\theta_i^2\rangle_0$, $D'=\langle\theta_i\theta_{i+1}\rangle_0$, $E=\langle\varphi_i^2\rangle_0$ (by symmetry $\langle\varphi_i\vartheta_j\rangle_0=0$), the SSWT amounts to set

$$\begin{aligned}\sin\theta_i\sin\theta_{i+1} &= \frac{1}{2}\big[\cos(\theta_i-\theta_{i+1})-\cos(\theta_i+\theta_{i+1})\big]\\ &\simeq e^{-D}\Big[(1+D)\sinh D' - D'\cosh D'\\ &\quad -\sinh D'\,\frac{\theta_i^2+\theta_{i+1}^2}{2}+\cosh D'\,\theta_i\theta_{i+1}\Big),\end{aligned}$$

and

$$\begin{aligned}\cos\theta_i\cos\varphi_i &= \frac{1}{2}\big[\cos(\theta_i-\varphi_i)+\cos(\theta_i+\varphi_i)\big]\\ &\simeq e^{-F}\Big(1+F-\frac{\theta_i^2+\varphi_i^2}{2}\Big),\end{aligned}$$

where $F\equiv(D+E)/2$ and we used the SSWT identity $\cos x \simeq e^{-\langle x^2\rangle/2}\big[1+\frac{1}{2}(\langle x^2\rangle - x^2)\big]$.

The SSWT Hamiltonian is diagonal in Fourier space:

$$\frac{\mathcal{H}_0}{J_{\rm c}} = -N e_0(t) + \sum_k \big[(A+B\,\mu_k)\,|\theta_k|^2 + C\,|\varphi_k|^2\big]\ , \quad \text{(B1)}$$

with $\mu_k = 1-\cos k$ and

$$\begin{aligned}A &= h\,e^{-F} - e^{-D-D'}\\ B &= e^{-D}\cosh D'\\ C &= h\,e^{-F},\end{aligned} \quad \text{(B2)}$$

while $e_0(t)$ collects the uniform contributions. It follows that the self-consistent expressions for the variances are

$$\begin{aligned}D &= \frac{t}{2N}\sum_k \frac{1}{A+B\,\mu_k} = \frac{t}{2\sqrt{A(A+2B)}}\\ D' &= \frac{t}{2N}\sum_k \frac{\cos k}{A+B\,\mu_k} = D - \frac{t}{2N}\sum_k \frac{\mu_k}{A+B\,\mu_k}\\ E &= \frac{t}{2\,C}\ .\end{aligned} \quad \text{(B3)}$$

The stability condition for $\mathcal{H}_0$ is $A\geq 0$, which defines a threshold field,

$$h_0(h,t) = e^{F-D-D'} < 1\ , \quad \text{(B4)}$$

above which the SSWT is meaningful. Note that the present approach can describe the finite-temperature behavior of the system also for $h \lesssim h_{\rm c}=1$, because the configuration density can still be approximated by a Gaussian centered in $\{\theta_i=0,\varphi_i=0\}$ as long as thermal fluctuations are large enough to overcome the barrier between the two symmetric minima $\theta_i = \pm\,\theta_{\rm m}$ of $\mathcal{H}$, as explained in Sec. III B.

From the SSWT Hamiltonian (B1) the Fourier transform of the correlation function is immediately found,

$$G_x(k) = \big\langle |\theta_k|^2\big\rangle_0 = \frac{t}{2(A+B\,\mu_k)}\ , \quad \text{(B5)}$$

and can be used to evaluate the correlation length ξ_x,

$$\xi_x^2 = -\frac{G_x''(k)}{2\,G(k)}\Big|_{k=0} = \frac{B}{2\,A} = \frac{e^{F-D}\cosh D'}{h-h_0(h,t)}\ . \quad \text{(B6)}$$

Therefore, when the field is close to the critical value $h_{\rm c}=1$, the behavior of the correlation length is given by $\xi_x \sim [h-h_0(h,t)]^{-1/2}$. In this region the variance D is enhanced ($A\sim 0$) and it can be easily seen seen that $D'\simeq D$ and $F\simeq D/2$, so that

$$\begin{aligned}\Delta(h,t) &\equiv 1-h_0(h,t) \simeq D+D'-F \simeq \frac{3}{2}D\\ &\simeq \frac{3\,t}{4}\big[(h-1+\Delta)(h+1+\Delta-D)\big]^{-1/2}\\ &\simeq c\ t\ (g+\Delta)^{-1/2}\ ,\end{aligned} \quad \text{(B7)}$$

with $g\equiv h-1$ and the constant $c=3/4\sqrt{2}$.

Rewriting this equation as

$$\frac{\Delta}{t^{2/3}} \simeq c\,\left(\frac{g}{t^{2/3}}+\frac{\Delta}{t^{2/3}}\right)^{-1/2} \quad \text{(B8)}$$

it appears that $\Delta/t^{2/3}=F(x)$, with $x=g/t^{2/3}$ and the asymptotic behaviors $F(0)=c^{2/3}$, $F(x\to\infty)\sim c\,x^{-1/2}$. From Eqs. (B6) and (B7) the leading behavior of the correlation length is given by

$$\xi_x \sim (g+\Delta)^{-1/2} \simeq t^{-1/3}\,F(x)\ , \quad \text{(B9)}$$

and it follows that near the critical point it is a homogeneous function,

$$\xi_x(b^2 g, b^3 t) \simeq b^{-1}\xi_x(g,t) \ , \qquad \text{(B10)}$$

which coincides with Eq. (23) with the exponents $\nu = 1/2$ and $y = 3$. For the crossover line (**bc**), identified by imposing $x \simeq 1$, one finds $t \sim g^{3/2}$.

[1] S. Chakravarty, B. I. Halperin, and D. R. Nelson, Phys. Rev. B **39**, 2344 (1989).
[2] M. A. Continentino, *Quantm Scaling in Many-Body Systems* (World Scientific, Singapore, 2001).
[3] D. Bitko, T. F. Rosenbaum and G. Aeppli, Phys. Rev. Lett. **77**, 940 (1996).
[4] H. M. Ronnow, D. F. McMorrow and A. Harrison, Phys. Rev. Lett. **82**, 3152 (1999).
[5] P. Carretta,T. Ciabattoni, A. Cuccoli, E. Mognaschi, A. Rigamonti, V. Tognetti, and P. Verrucchi, Phys. Rev. Lett. **84**, 366 (2000).
[6] H. M. Ronnow, R. Parthasarathy, J. Jensen, G. Aeppli, T. F. Rosenbaum, and D. F. McMorrow, Science **308**, 389 (2005).
[7] S. Sachdev, *Quantum phase transitions* (Cambridge University Press, Cambridge, UK, 1999).
[8] S. Katsura, Phys.Rev. **127**, 1508 (1962).
[9] P. Pfeuty, Ann. Phys. **57**, 79 (1970).
[10] L. Onsager, Phys. Rev. **65**, 117 (1944).
[11] Note that, according to the standard notations used in Eq. (1), the dimensional factor $\hbar$ of the spin angular momenta is embodied in $J \propto \hbar^2$ and in $H \propto \hbar^{-1}$; therefore, taking the classical limit $S \propto \hbar^{-1} \to \infty$, these limits are well defined; see, e.g., J. Oitmaa and G. J. Coombs, J. Phys. C **14**, 143 (1981).
[12] T. Horiguchi, J. Phys. Soc. Japan **9**, 3142 (1990).
[13] K. Minami, J. Phys. A **29**, 6395 (1996).
[14] K. Minami, J. Phys. Soc. Japan **67**, 2255 (1998).
[15] L. Amico, D. Patanè, Europhysics Lett. **77**, 17001 (2007).
[16] A. Taiti *Tesi di Laurea* (Università di Firenze, 2006).
[17] M. Blume, P. Heller, and N. A. Lurie, Phys. Rev. B **11**, 4483 (1075).
[18] M. Abramowitz and I. A. Stegun, *Handbook of mathematical functions* (Dover, new York, 1964).